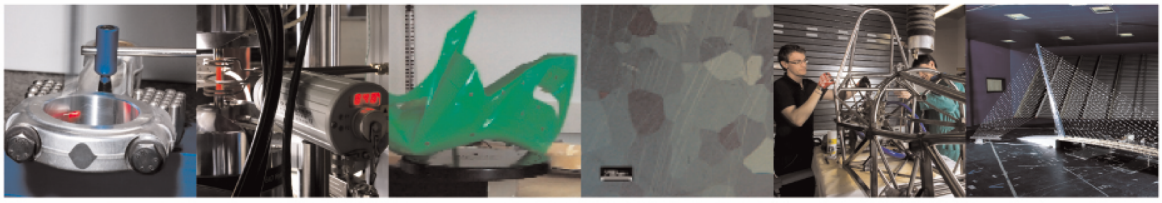

Distributed fibre optic monitoring of mode I fatigue crack propagation in adhesive bonded joints and comparison with digital image correlation

R. A. A. Lima, F. Migliavacca, L. M. Martulli, M. Carboni, A. Bernasconi

This is a post-peer-review, pre-copyedit version of an article published in Theoretical and Applied Fracture Mechanics. The final authenticated version is available online at: https://doi.org/10.1016/j.tafmec.2022.103501

DIPARTIMENTO DI MECCANICA ■ POLITECNICO DI MILANO
via G. La Masa, 1 ■ 20156 Milano ■ EMAIL (PEC): pecmecc@cert.polimi.it
http://www.mecc.polimi.it
Rev. 0

Distributed fibre optic monitoring of mode I fatigue crack propagation in adhesive bonded joints and comparison with digital image correlation

R. A. A. Lima, F. Migliavacca, L. M. Martulli, M. Carboni, A. Bernasconi[1]

Dept. Mechanical Engineering, Politecnico di Milano, Milan, Italy

The feasibility of applying Optical Backscatter Reflectometry as a backface strain monitoring method for bonded joints subjected to mode I fatigue crack propagation was studied. Visual evaluation and Digital Image Correlation methods were applied to track the crack-tip position and the onset of plasticisation in the adhesive, respectively. The methods were compared to understand the relationship between the changes in the optical fibre measurements and the crack propagation. The absolute maximum strain values gave important information about the crack propagation stage (stable or high velocity) within the adhesive and fast-rate crack propagation, which resulted in a sudden increase in strain values. Finally, the strain peak position was found to be a valuable indicator of crack tip position.

Keywords: adhesively bonded joints, fatigue crack propagation, distributed strain sensing, optical fibres, digital image correlation

[1] Corresponding author: e-mail: andrea.bernasconi@polimi.it (A. Bernasconi).

1. INTRODUCTION

Adhesively bonded joints are a promising option for mechanical joining in lightweight structures thanks to several advantages they offer: less weight to high strength ratio, a more even stress distribution in multi-materials joining, and excellent design flexibility [1]–[3]. Methods for controlling their in-service reliability are required to ensure the extensive use of adhesively bonded joints in primary structures.

Structural Health Monitoring (SHM) methods are solutions to in-service structural damage diagnosis (identification, localisation and quantification) and remaining useful life prognosis. SHM methods can be based on the identification of different physical phenomena such as the propagation behaviour of elastic waves [4]–[7], changes in modal data as frequency values and shape [8], [9], propagation of acoustic emission waves in materials under deformation or damaging mechanisms [10]–[16], variation in electromechanical impedance [17]–[21] and static parameters (temperature, strain and displacements) [22]–[28].

Amongst several promising techniques for monitoring the structural integrity of adhesively bonded joints under quasi-static [22], [29]–[34] and fatigue loading conditions [19], [35]–[39], backface strain measurements are widely used in the literature. This method generally uses an array of discrete and punctual sensors (e.g., strain gauges or optical fibres equipped with Bragg gratings) installed onto the joints' external surface to assess variations in their strain profiles. Consequently, since damage propagation within bonded joints modifies their stiffness and their strain responses, these methods can be used for damage monitoring [17], [26], [41]–[45].

Optical Fibres (OFs) are particularly suitable for backface strain measurement due to their low invasiveness, long-term stability also under fatigue loading, electromagnetic invulnerability and great accuracy [23], [45]–[47]. Fibre Bragg Gratings (FBG) and Chirped Fibre Bragg Gratings (CFBG) are the most commonly used OF sensors, allowing strain measurements to be done punctually (as a strain gauge) or in a distributed manner (over the sensor's length), respectively [34], [37], [48]–[52]. Furthermore, the Optical

Backscatter Reflectometry (OBR) technique allows strain measurements over long distances, and it transforms the OF into a high spatial resolution distributed sensing unit [32], [50], [53]–[55].

The OBR technique measures stochastic local modifications in the OF refractive index, using swept wavelength interferometry, due to changes in its Rayleigh backscattering, triggered by inherent core defects. As each fibre presents different core defects, a fingerprint for each fibre's Rayleigh backscatter pattern must be derived [55]–[58]. Changes in the fibre's refractive indexes are observed when it undergoes external temperature and/or mechanical strain stimuli, so mechanical and thermal strains' variations can be evaluated point-by-point by comparing the new pattern with the reference fingerprint [39].

OBR distributed sensing applied to backface strain measurement was studied elsewhere [32] to monitor crack propagation within metallic adhesive joints under quasi-static mode I loading conditions. OBR results were compared with Digital Image Correlation (DIC) and visual evaluation measurements to track the crack-tip position within the adhesive. The investigated adhesive showed ductile behaviour and a non-negligible fracture process zone. DIC could identify the adhesive's onset of plasticisation, while visual evaluations determined the position of the crack tip. Furthermore, variations in the position of the absolute strain peaks, measured by OBR, were compared with the various techniques. It was concluded that, for the studied adhesive under cohesive crack propagation, OBR results coincided with DIC ones, suggesting that the strain peak positions assessed by the OBR represent the beginning of the fracture process zone within the adhesive.

This promising result could open new perspectives for in-service fatigue monitoring. Fatigue crack monitoring of adhesively bonded joints using the OBR technique was indeed evaluated as an SHM method in the literature [39]. However, no special attention was given to the relationship between the OBR results and the mechanical behaviour of the adhesive itself. Moreover, using a mixed-mode specimen like the single lap joint prevented a detailed study of the damage evolution within the adhesive. Finally, the studied joint had composite adherends that could promote different damage mechanisms within the

composite (i.e. matrix cracking and delamination). Overall, a deeper analysis was deemed necessary and this led to adopting OBR distributed sensing to monitor fatigue damage propagation in metallic Double Cantilever Beam (DCB) bonded joints with a toughened adhesive.

The present work focuses on monitoring mode I fatigue crack propagation by OBR. DIC and visual evaluation are also applied to identify and possibly measure the crack tip position and to assess the presence of a non-negligible process zone. The measured backface strain profiles and their positions are then evaluated, and their relationship with the joint's actual fatigue behaviour is discussed. Finally, the OBR outcomes assessed during the fatigue tests are compared with the quasi-static ones.

2. MATERIALS AND METHODS

2.1. Materials and samples fabrication

The high strength steel DIN 40CrMoMn7 was used for the adherends. The adhesive was a bi-component 3M Scotch-weld^{TM} 7260B/A Non-sag epoxy adhesive, whose mechanical properties are described in [59], [60]. The DCB sample's main dimensions were chosen in agreement with the ASTM D3433 standard and are detailed in Figure 1.

First, the adherends were sandblasted to achieve a rough and uniform surface. After that, their surfaces were cleaned with acetone. Finally, the adhesive was mixed and applied with a mixing nozzle attached to a hydraulic applicator. Glass microspheres with 300 μm were added to the adhesive layer with a concentration of 2% by total adhesive weight to ensure a minimum bondline thickness of 0.3 mm. A razor blade was fixed at the beginning of the bondline to ensure a sharp crack tip at the beginning of the tests.

The specimens underwent a polymerisation cycle in an oven. The cycle was divided into three main steps: a linear temperature increase from room temperature to 65°C for 1.5 hours, then a constant temperature stage at 65°C for 3 hours and, finally, cooling to room temperature for 1 hour. Two specimens (S1 and S2) were manufactured.

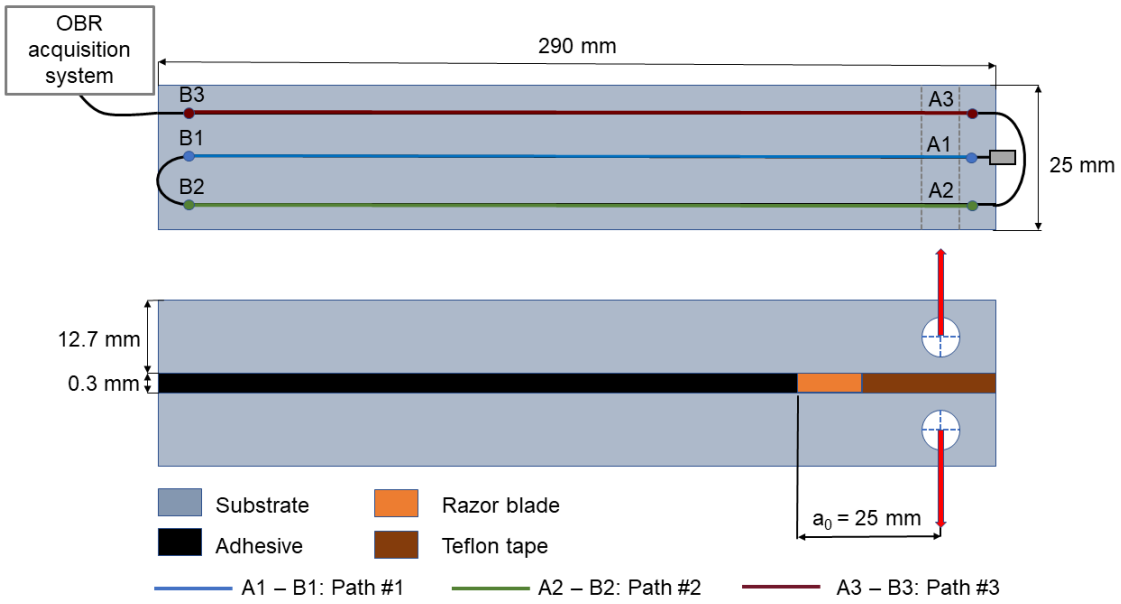

Figure 1: DCB dimensions and optical fibres layup (Drawings not to scale).

After curing, both DCBs lateral surfaces were cleaned to remove excess adhesive. They were then white painted with water-based paint to improve crack contrast for the visual evaluation method. A random speckle pattern was then painted on one of the specimens' lateral surfaces by spraying arbitrary shaped aerosol stains of black paint. This was required for DIC measurements. Finally, a paper ruler was bonded on both lateral surfaces to aid the crack-tip visual tracking.

High-definition optical fibres supplied with LC/APC connectors were bonded on the samples' bottom part. First, the samples' surfaces were cleaned using acetone. Then, the fibres were carefully placed following the layout described in Figure 1 and kept in place with adhesive tape; fibres have to be carefully handled because they are brittle, have a 200 µm diameter and possess low shear strength. Finally, the optical fibres were bonded using the X60 bi-component epoxy adhesive (supplied by HBM Company, Germany) [32].

2.2. Fatigue cracking propagation procedures

Fatigue crack propagation tests were performed in load control mode. A constant amplitude cyclic tension-tension load was applied with a sinusoidal shape, and the fatigue ratio (minimum load / maximum load) was set to R = 0.1. A uni-axial MTS 810 servo-hydraulic machine equipped with a load cell of 15 kN was used. The peak load was set to 1950 N to achieve an initial G_I value of 0.2 N/mm^2 (see section 2.3), and a testing frequency of 5 Hz was applied. No additional pre-cracking stage was performed, assuming that a sharp crack tip was ensured by the razor blade.

Fatigue crack propagation tests were stopped every 5000 cycles to perform a monotonic loading ramp, with a speed rate of 0.5 mm/min, up to the maximum fatigue load. Once the maximum load was reached, it was held for 10 seconds, and visual evaluation, DIC and OBR measurements were acquired to investigate damage evolution. Then, the load was decreased to the minimum value of the cyclic loading condition. The testing setup is shown in Figure 2. Tests were conducted until the specimen's complete failure or crack propagation exceeded the width of the field of view (100 mm) of DIC.

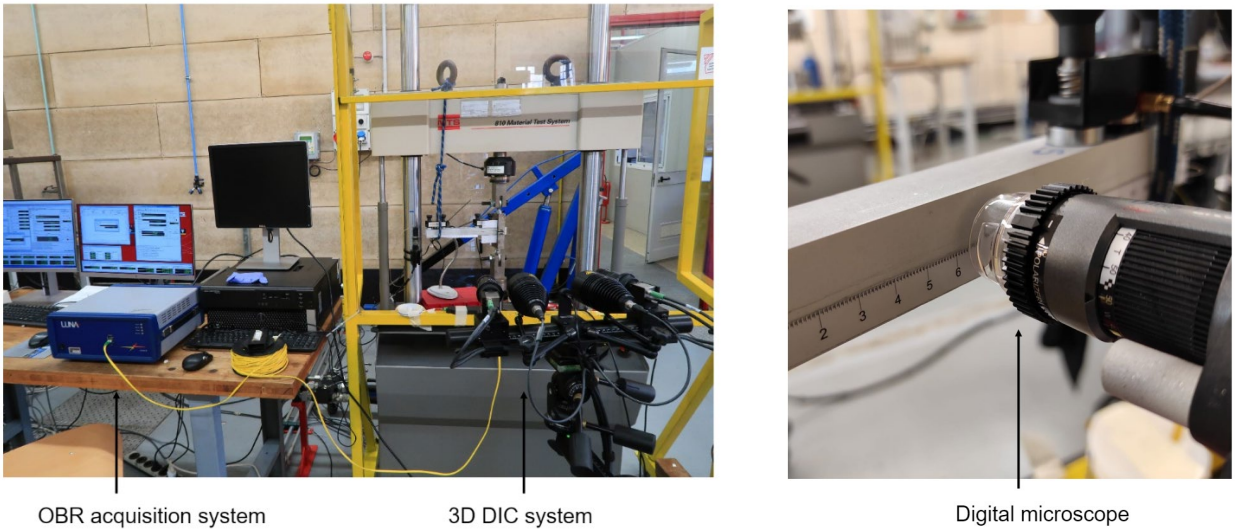

(a) (b)

Figure 2: Fatigue crack monitoring setup.

2.2.1. Fatigue crack monitoring setup

Crack initiation and propagation were monitored using three main techniques: visual evaluation, DIC and OBR.

Visual evaluation was performed using a high magnification Dino-Lite digital microscope, incorporated with an LED system, and supported by a flexible gooseneck stand, as recommended by the ISO 25217 standard. With a magnification of 20x, the digital microscope took pictures of the white-painted samples' lateral surface during the maximum ramp load, as detailed in Figure 2 (b).

DIC was performed using the GOM – 3D Aramis adjustable system using an acquisition frequency of 3 Hz. The Aramis system included two cameras of 12 Megapixels resolution, adjustable dual-LED lights (10°) and post-processing software (GOM correlate – version 2020). The camera lenses were Titanar B 75 mm type with 22 mm of aperture and 25° of stereo angle, resulting into a field of view 110 mm wide and a 39 pixels/mm image scale.

Before the tests, a calibration of the DIC system was needed. A CP 40/MV panel, positioned at a specific stand-off distance of 697 mm, was used to adjust image distortions and temperature changes. After that, a calibration deviation factor of 0.03 pixels was found. The DIC acquisition system had the images synchronised with load and displacement outputs from the testing machine. For the post-processing stage, a Region of Interest (ROI) was defined with a subset and step sizes equal 33 and 11 pixels.

OBR was applied for the backface strain measurements. The optical fibres were connected to an OBR ODiSI-B interrogator supplied by Luna Innovations Inc. (Virginia – USA), capable of acquiring and processing the Rayleigh backscatter radiation within the fibre and converting it into a strain profile. The Luna interrogation system allows for the optical fibre to be used as a distributed sensor ofhigh spatial resolution. For the performed tests, virtual sensors with a gauge length of 1.3 mm and a pitch of 0.65 mm between adjacent sensors were selected.

During loading ramps at fatigue test interruptions, the strain response was continuously acquired using a frequency of 5 Hz. Then, at the maximum load of the monotonic ramps, all the acquired strain measurements were 10-sampling moving averaged in time (every 1 second) to reduce noise. The DIC acquisition was done during the entire loading ramps with a frequency of 3 Hz.

Since OFs are also sensitive to temperature changes, the length of each optical fibre path bonded on the bottom surface of the DCB samples was determined by positioning a hot source next to the OF paths' edges, as described in [32]. Once the paths' lengths were defined, it was possible to separate only the regions of interest and analyse the strain response of each single path.

It is worth mentioning that, before starting the fatigue test on sample S1, a baseline acquisition was carried out to identify the bondline initial position, in the undamaged specimen, along the optical fibre.

3. RESULTS

3.1. Fatigue crack propagation tests

Both specimens presented a similar behaviour during fatigue crack propagation tests, and the tests were interrupted every 5000 cycles for OBR, DIC and Visual evaluation data acquisition. The final interruption was done at 45000 cycles for specimen S1 and at 40000 cycles for specimen S2.

In general, a predominant cohesive failure was observed in both specimens. However, at the beginning of the tests, a region of adhesive failure was observed (see the red squares in Figure 3), which is more prominent in sample S1 than in sample S2. Sample S2 failed during the test, while the test on sample S1 was interrupted before reaching the final failure and it was fully opened by applying a quasi-static loading until separation. This caused differences in the fracture surfaces of specimen S1 (the dark grey area corresponding to the fatigue propagation and the light grey area to the quasi-static one).

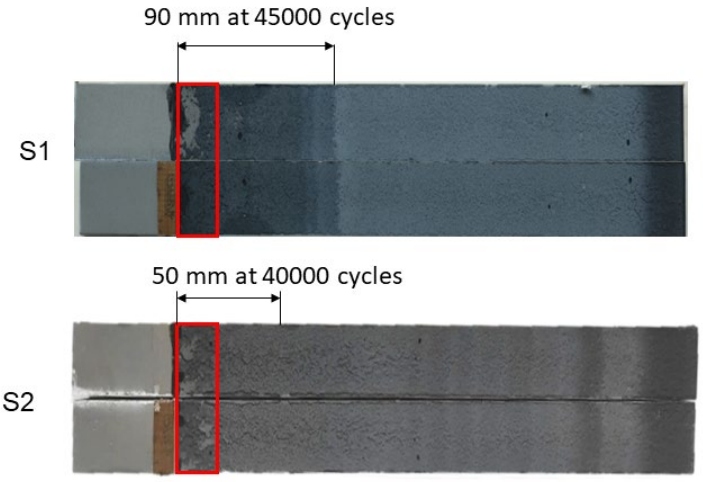

Figure 3: Fracture surface of specimens S1 and S2 after the fatigue crack propagation tests.

3.2. OBR results

Figure 4 shows the backface strain distribution measured by OF, on sample S1, at the beginning of the test (baseline) and after 40000 fatigue cycles. The negative strain peaks are caused by the stress concentration at the beginning of the specimen's bondline. The peak position corresponds to the razor blade's tip at the beginning of the test and, as soon as the crack propagates, to the advancing position of the crack front. As both samples presented similar results, only the strain profiles measured on sample S1 are described in this section unless otherwise stated.

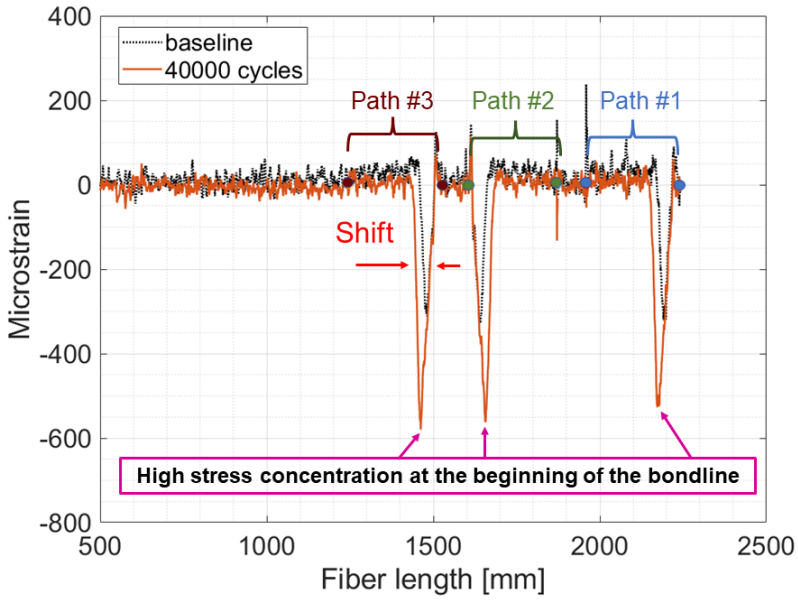

Figure 4: Optical fibre strain distribution at baseline and after 40000 cycles (sample S1).

First, higher absolute values of strain peaks can be observed after applying fatigue loading. This is caused by damage development that makes the specimen less stiff, as reported in [27], [42], [23], [54].

Moreover, a shift in the position of strain peaks along the optical fibre can be noticed. As mentioned earlier, this could represent either the onset of the adhesive's process zone, as was observed during mode I quasi-static tests of the same joint type [32], or the position of the crack tip [27], [54].

Figure 5 (a) shows the baseline strain profile outputs of the three paths. It can be observed that the strain peaks are very close to each other, suggesting a uniform and straight crack front (razor blade position) through the specimen width. It is worth mentioning that the strain profiles presented in Figures 5 (a) and (b) were rectified for clarity.

Figure 5 (b) shows the exemplificative case of the strain measured along Path #2 of the optical fibre as a function of the number of cycles (the other paths showed similar results). As observed, the strain peak shifts as the number of cycles increases. The maximum strain

values undergo a slight increase until 30000 cycles, while, especially for sample S1, a significant increase from 300 με to 1250 με in the absolute strain values was noticed after 35000 cycles.

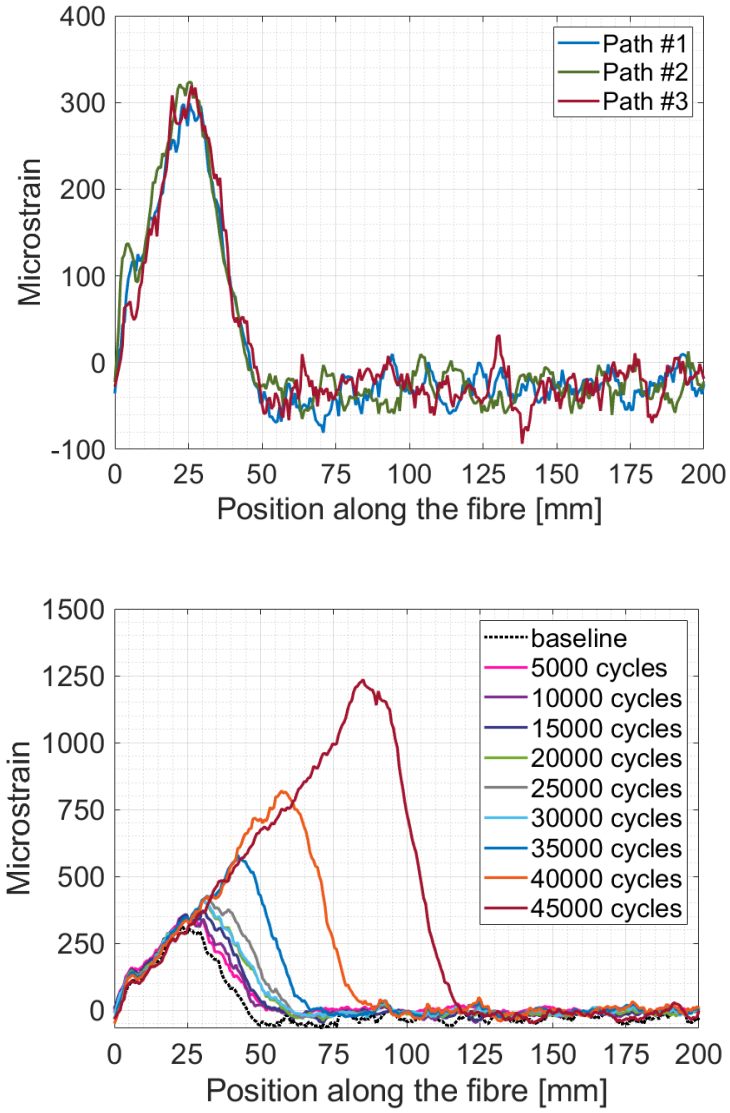

Figure 5: Sample S1: (a) Strain profile representation of the three optical fibre paths during the baseline acquisition and (b) strain profile representation of Path #2 as the function of the number of applied fatigue cycles.

Figure 6 (a) showcases the absolute value of the strain peaks of all the three paths versus the number of cycles for both specimens, while Figure 6 (b) showcases the strain peak values of Path #2, for both specimens, as a function of their position along with the specimens. The peak position reported in Figure 6 (b) is measured from the loading point.

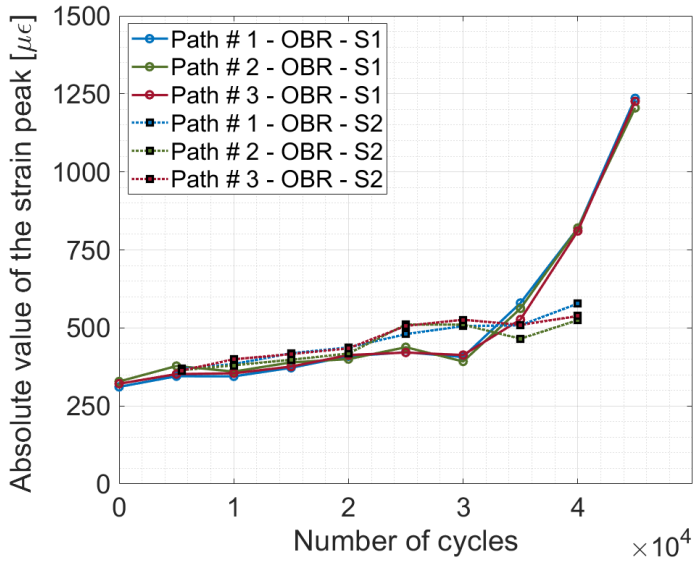

(a)

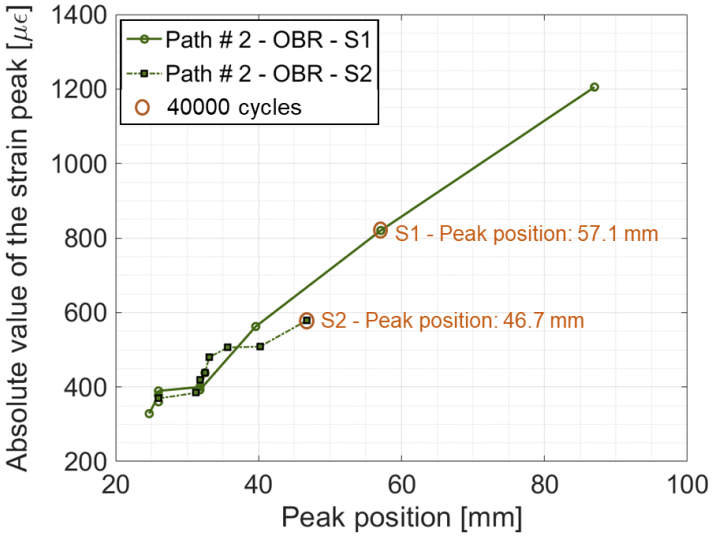

(b)

Figure 6: (a) Maximum absolute strain values versus the number of cycles for both specimens and (b) maximum strain values of Path #2 as a function of peak position.

Sample S2 showed a lower increase than sample S1 in the maximum strain values, from 300 με to about 500 με. Moreover, sample S2 had a sudden failure after the interruption of 40000 cycles. Sample S1, instead, did not fail during the test, which was interrupted after 45000 cycles because the crack length exceeded the ROI of DIC.

The lower absolute strain values of sample S2 can be better understood by looking at Figure 6 (b), in which the orange circles represent the OBR measurements at 40000 cycles. Sample S2 presents a maximum absolute strain value of around 600 με for a crack length, assessed by OF, of about 46.7mm. Therefore, the crack was shorter than the one observed in specimen S1, for which a 57.1 mm crack length and an 800 με peak strain were recorded at the same number of cycles. Being the tests performed in load control mode, higher values of the backface strain in the specimens' arms are expected for longer crack lengths, as shown in [39].

3.3. Visual evaluation and DIC measurements

Crack estimations by visual evaluation and DIC were done by post-processing the images taken during the hold time at maximum load, at the end of the monotonic ramps. The open-source software Image-J (version 2) was used to measure the crack length within the joints after each fatigue test interruption. The crack length was evaluated as the distance between the initial crack length of the undamaged specimen (zero of the ruler and razor blade position) and the crack-tip position detected in the analysed frame.

GOM Correlate (version 2020) was used as post-processing software for DIC acquisitions. First, virtual extensometers were created to obtain the DCB adhesively bonded joints' total opening displacement [15], [32]. It was then possible to identify two significant regions in the opening displacement curves of each frame: a zone with negligible variations in the opening displacements and a region with significantly higher displacement values, as well-detailed in [32], [62]. The transition point between areas is defined as the "DIC opening

point", which is determined as the first point where the displacement values are higher than a pre-calculated threshold, as described in [15], [32] and shown in Figure 7.

For quasi-static mode I tests of the same adhesive as the one studied in this work, the "DIC opening point" represented the adhesive's onset of plasticisation [32]. Moreover, the distance between the visual evaluation measurements (crack-tip position) and the DIC opening points proved to be the adhesive fracture process zone length [63].

Using DIC analysis, Sun and Blackman [64] proposed an automated method to measure the crack length in DCB adhesively bonded joints. Winkler's elastic foundation model was applied to describe the vertical displacement of symmetric DCB samples mathematically. One substrate can be considered a beam laying on an elastic foundation (see Appendix A), and its deformation tends to zero far from the crack tip [65].

Sun and Blackman method could identify the following regions in the DCB specimens (Figure 8):

1. the onset of plasticisation in the adhesive, defined as the point of the vertical displacement curve where it gets equal to zero, i.e. at the transition between the tension and compression regions;
2. a compression region due to adherends' rotation near the crack-tip;
3. an undamaged region.

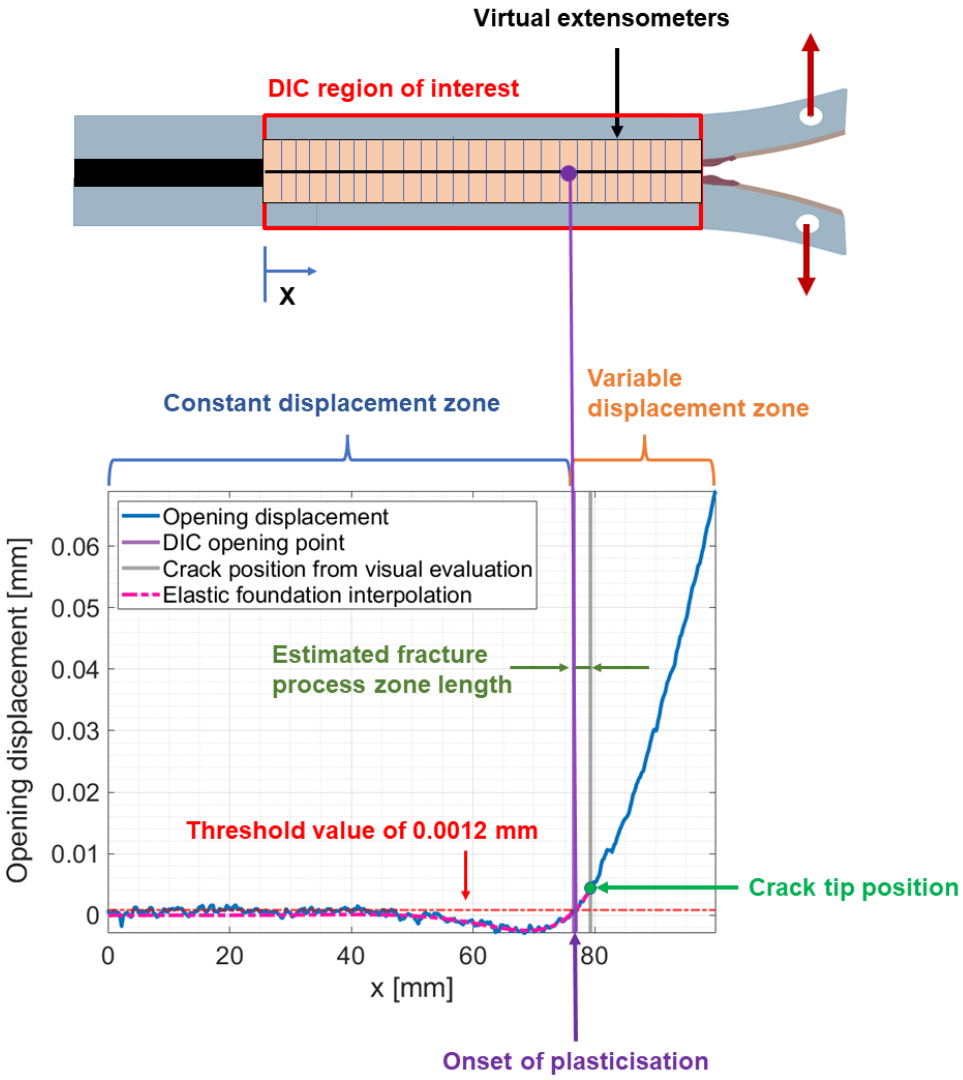

Figure 7: DIC opening point determination and visual measurements.

Figure 8 compares the position of the DIC opening point to that of the onset of plasticisation point obtained by Sun and Blackman method. The crack-tip position was defined by the visual evaluations from one of the sample's lateral surfaces. It appears that the elastic foundation interpolation suggested by Sun and Blackman [66] perfectly matches the opening displacement obtained by the virtual extensometers' measurements.

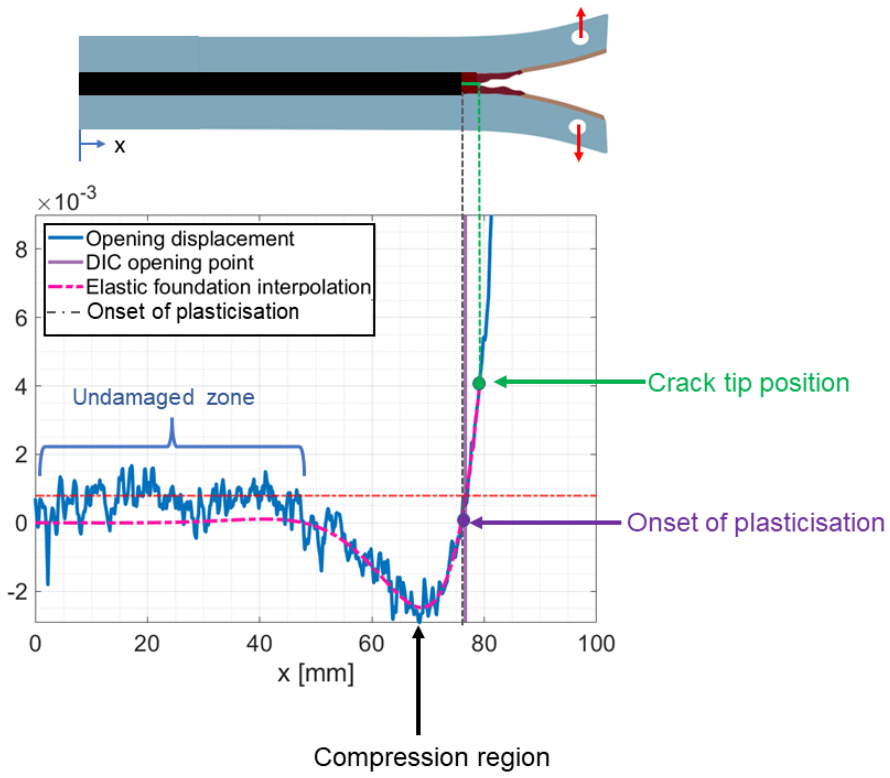

Figure 8: Comparison between DIC opening point determination and comparison with elastic foundation interpolation.

The transition point between the constant displacement region and the negligible displacements (DIC opening point), provided by the elastic foundation interpolation and the opening displacement method, is almost the same, with a difference of about 0.1 mm. This result confirms that the physical meaning of the DIC opening point is the onset of the fracture process zone in the studied adhesive subjected to fatigue loading. Furthermore, the compression and undamaged regions (region of constant displacement) could also be identified.

4. DISCUSSION

4.1. OBR results compared with visual evaluation and DIC measurements

As observed previously, the strain peak position assessed by the optical fibres indicates the position of the damage front in adhesively bonded joints [32]. The position of the strain peak of each OBR curve was thus compared with the visual evaluation and the DIC measurements, as shown in Figure 9.

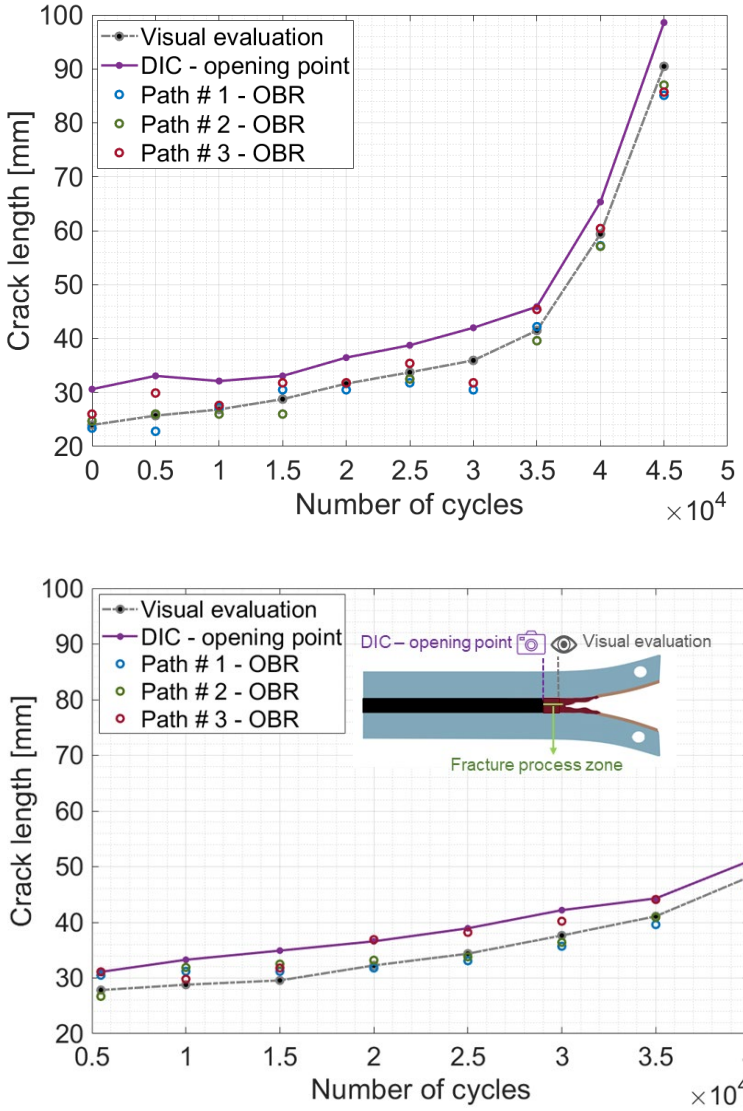

Figure 9: Comparison between visual evaluation, DIC opening point measurements and OBR peak positions (a) sample S1 and (b) sample S2.

As already mentioned, the DIC opening point captures the onset of plasticisation, while visual evaluation captures the fracture in the adhesive; thus, the distance between them indicates the Fracture Process Zone (FPZ) [15], [32], [63], [64]. It can be observed that the considered adhesive has a non-negligible FPZ under fatigue loading conditions. During the steady-stable crack propagation stage of the fatigue tests, its length is about 4 mm, while in the final stage of the test, where a high-speed crack propagation was observed, it is about 2 mm. Even if counterintuitive, the authors associate this difference in the estimated fracture process zone length with the change from a stable to a high-speed crack propagation phase, possibly indicating a nonlinear behaviour in this stage, as stated in [19], [67]. Nevertheless, a deeper analysis focusing on the plastic behaviour of the adhesive would be required to fully explain this outcome and it is proposed as a future development.

The OBR peak positions almost coincided with the visual evaluation measurements, identifying the crack-tip position within the adhesive during the fatigue tests, as can be seen in [26], [41] - [43]. This aligns with Khoramishad et al. [75], who observed correspondence between experimental and numerical backface strain measurements with the visual crack-tip length under fatigue loading.

No significant differences in the measurements of the optical fibre's paths were found for both specimens, except for the second and fourth load ramps (5000 and 15000 cycles) of sample S1. This can be explained by a non-uniform crack front propagation due to adhesive failure at the first stages of crack propagation in sample S1, as already anticipated in Section 3.1 and Figure 3 and better shown in Figure 10.

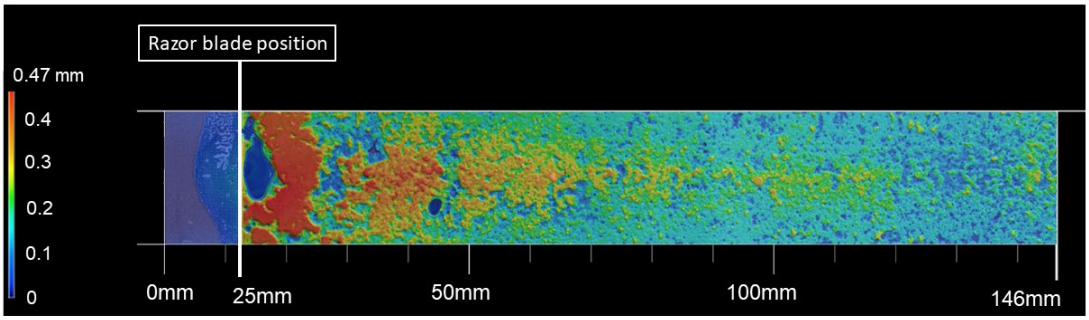

Figure 10: Topography map of sample S1.

Figure 10 shows the 3D topography of one of the two adherends of sample S1, made using the microscope Keyence VR-3500 available at the Department of Aerospace Structures and Materials of TU Delft (the Netherlands). The colour bar values indicate the adhesive layer's estimated height (z coordinate). The zero value (dark blue) was set at the adherend's free and clean surface. A fully cohesive failure is assumed to correspond to depths between 0.1 and 0.2 mm (between turquoise and green colours). Dark blue areas within the bonded area should correspond to fully interfacial failure or lack of adhesive. The dark orange and red colours should represent the largest distance from the adherend's surface, indicating a local adhesive failure of the sample originating from the opposite adherend's surface.

It is worth mentioning that the maximum height value measured by 3D topography (0.47 mm) differs from the nominal diameter of the glass beads (0.3 mm) used to control the bondline thickness. Larger values can be explained as the effect of the overflow of the adhesive under and above the razor blade, clearly visible in Figures 3 and 10, which may have caused an increase in the bondline thickness on the razor blade's side. Part of the difference could also be ascribed to the plastic deformation of the adhesive.

From 25 to 55 mm, the fracture surface is rougher than the final part of the test, indicating that the crack propagation plane changes throughout the adhesive's thickness. Conversely, in the region from 55 to 100 mm (faster crack propagation), a progressively smoother surface was observed with propagation in the adhesive's mid-plane and fewer changes in the crack propagation plane.

A quantitative comparison, by confidence analysis, between OBR peak positions, visual evaluation and DIC measurements is proposed in Figure 11.

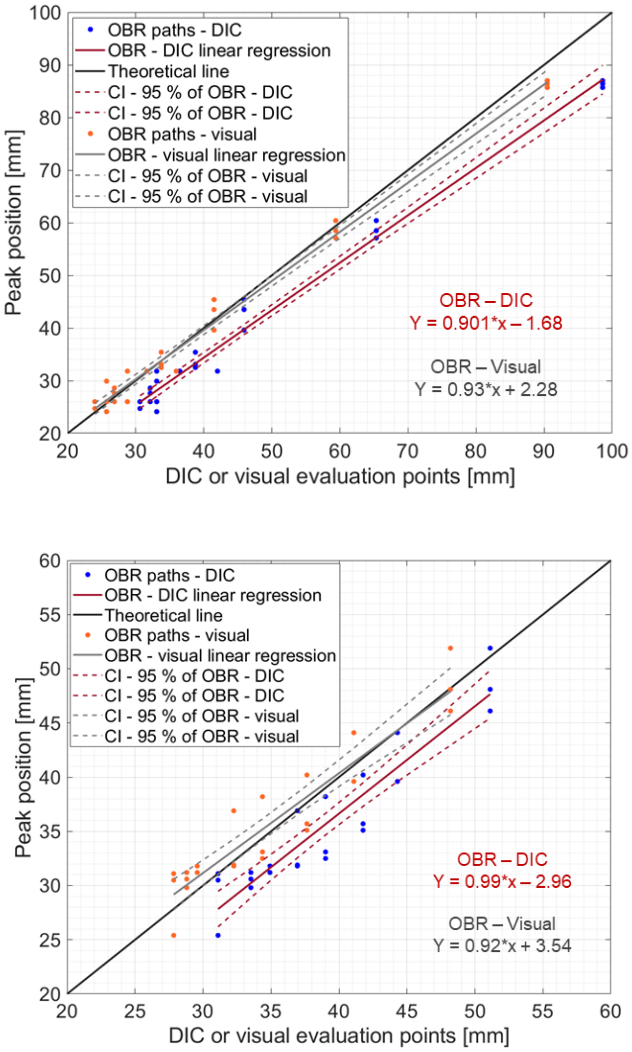

Figure 11: Confidence analysis of OBR peak positions and crack length measured by DIC and visual evaluation during fatigue tests for samples (a) S1 and (b) S2.

In Figures 11 (a) and (b), the black line represents the ideal 45° trend line for the correlation between data. The grey line reports the confidence analysis of the correlation between OBR strain peak positions and the crack length measured by the visual evaluations. A good match between OBR and visual measurements of the crack propagation for both specimens is observed.

However, for sample S1, a larger distance from the interpolating OBR-DIC and the theoretical line is observed at the end of the curve (cracks longer than 70 mm) with an average vertical offset between them of around 9 mm. On the other hand, the vertical distance between the OBR-Visual and the theoretical line at the end of the curve was around 2.5 mm. Increases in fatigue crack propagation rate can explain this increment in the average vertical offset between the lines. However, the same behaviour could not be observed in sample S2 because the measurements were taken only during the stable crack growth phase, as discussed in section 3.2.

For the studied adhesive, under fatigue loading, the OF maximum strain peaks position can thus be associated with the position of the crack-tip measured by visual evaluation, at least for the crack growth rates considered in this study. Therefore, the OBR appears to be a promising method for monitoring crack-tip propagation in adhesively bonded joints under mode I fatigue loading.

4.2. Comparison between OBR results of DCB specimens under quasi-static and fatigue mode I loading conditions

The monitoring of quasi-static mode I crack propagation in metallic adhesively bonded DCB joints using the OBR distributed sensing method was previously studied [32]. In addition, DIC and visual evaluation were also used to track the crack-tip propagation.

It was concluded that, for cohesive crack propagation in quasi-static tests, the OBR strain peak position presented results very similar to those obtained by DIC, suggesting an identification of the adhesive's onset of plasticisation. Even with not completely cohesive

crack propagation, the OBR output fell between the DIC and Visual evaluation measurements (crack-tip position).

It is worth mentioning that with the adhesive 3M 7260 B/A the size of the quasi-static FPZ was equal to about 10 mm. On the other hand, the FPZ under fatigue loading was about 40% smaller than the quasi-static case. This can be explained considering that the FPZ length depends on the magnitude of the applied load: the applied fatigue load was 20% of the static one, thus resulting in a smaller FPZ [68], [69], [70].

The main differences observed between the fatigue and quasi-static tests are described below:

- under fatigue loading, OBR observations are closer to visual evaluation than DIC measurements (small FPZ length). The opposite occurred for the quasi-static load. The reduced applied maximum load can explain this trend, as demonstrated in [69], [71];
- another relevant phenomenon in adhesives under fatigue loading conditions is "plasticity-induced crack closure" [68], [69], [72], [73]. This phenomenon is predominant in adhesives displaying a ductile behaviour. At the minimum load levels of the fatigue loads, the previously opened crack surfaces close and get in touch prematurely due to the onset of the so-called “plastic wake” [68], and this localised crack closure reduces the tensile stresses ahead of the crack tip. This could suggest that the onset of plasticisation in the adhesive, under fatigue loading, is not the point of maximum backface strain. However, further studies are needed to deepen this point;

- the optical fibres allowed for a sudden increase in the OBR strain peaks to be recorded during the final crack propagation stage of the fatigue tests. Conversely, the strain peaks’ absolute value remained almost constant under quasi-static loading. Therefore, the variations in the strain values measured by the backface monitoring technique can be interpreted as an indicator of fast crack growth rates.

Finally, the OBR measurements could effectively monitor damage propagation under quasi-static and fatigue loading. However, the strain peak position shifts represent the crack tip growth for the fatigue loading condition, while, on the other hand, they mainly represented the onset of plasticisation within the adhesive for the quasi-static condition.

5. CONCLUDING REMARKS AND FUTURE WORKS

The feasibility of using the shifts of Optical Backscatter Reflectometry backface strain peaks as a fatigue crack monitoring method of adhesively bonded DCB was studied. Results were compared with visual evaluations and the DIC opening point method. From the obtained results, the following conclusions can be drawn:

- Optical Backscatter Reflectometry can be used to obtain the backface strain profile of the DCB adhesively bonded joints under mode I fatigue loading conditions. Moreover, the optical fibres strain peak shifts are useful for identifying crack propagation;
- for mode I fatigue loading conditions, the strain peak positions monitored by the optical fibres correspond to the crack-tip position within the adhesive, with an excellent agreement with the visual evaluation points. This outcome differs from the quasi-static ones, where the OBR measurements located the adhesive's onset of plasticisation;
- despite the differences in the physical meaning of the OBR measurements, the method could still effectively monitor the bonded joint's structural integrity by identifying the crack tip under fatigue loading.

Finally, OBR displayed promising characteristics to be implemented for in-service damage measurement in real-time or on-demand.

A possible development of this work regards the feasibility of using the OBR technique to determine the crack-tip position in bonded joints under mode II and mixed-mode. Sourisseau et al. 2022 [74] installed optical fibres onto ENF and Mixed-Mode Bending

(MMB) specimens at two different positions: on the outer surface of one adherend and embedded in the bondline. Quasi-static tests were then performed and strain profiles were recorded by the OBR technique. It was observed that the position of the maximum strain peak assessed by the optical fibres could be associated with the crack tip position for both cases. It would thus be interesting to evaluate the effectiveness of this technique also under mode II and mixed-mode fatigue loadings.

6. ACKNOWLEDGEMENT

Support by the Italian Ministry for Education, University and Research through the project Department of Excellence LIS4.0 (Integrated Laboratory for Lightweight e Smart Structures) is acknowledged.

The authors would like to thank Prof. Sofia Teixeira de Freitas and Dr. Ran Tao (both at the Department of Aerospace Structures and Materials of TU Delft, the Netherlands) for the help in pursuing the fractography analyses of the studied samples.

7. APPENDIX A

Sun and Blackman [64] proposed an automated method, based on the Winkler's elastic foundation model, to determine the position of the onset of plasticisation within an adhesive under mode I quasi-static tests by using the DIC opening curve measurements. The opening displacement of the DCB specimen (w), considered as one adherend laying on an elastic foundation was described by Equation 1.

$$w(x) = (\sqrt{B_1^2 + B_2^2}) * e^{-\lambda x} * \cos(\lambda x - \varphi)\, x \geq 0 \qquad \text{Eq. 1}$$

where φ is the phase angle defined in Eq. 2 and B_1, B_2, described in Eq. 3, Eq. 4 and Eq. 5, respectively.

$$\varphi = tan^{-1}\left(\frac{B_2}{B_1}\right) \quad \text{Eq. 2}$$

$$B_1 = P * \left(\frac{2\lambda}{k}\right) + (P * a_0) * \left(\frac{2\lambda^2}{k}\right) \quad \text{Eq. 3}$$

$$B_2 = -(P * a_0) * \left(\frac{2\lambda^2}{k}\right) \quad \text{Eq. 4}$$

$$\lambda = \left(\frac{k}{4EI}\right)^{1/4} \quad \text{Eq. 5}$$

In Eq. 2-5, P is the load applied during the test, a_0 length of the crack tip, k is a constant that for symmetric DCB specimens can be defined as $k \approx Eb/h$, E is the adherent's elastic modulus, I is the beam's second moment of area, b and h are the adherent's width and thickness, respectively.

The opening displacement was determined by GOM correlate software, where an opening displacement curve was obtained for each fatigue test interruption. From regression analysis of the opening displacement curves and solving Equation 1, it was possible to determine the independent variables B_1, B_2 and λ by Matlab fitting tool (version 2021). After that, the position of the onset of plasticisation within the adhesive could be evaluated by Eq. 6.

$$x_{onset} = \frac{tan^{-1}(1 + 1/\lambda * a_0)}{\lambda} \quad \text{Eq. 6}$$

REFERENCES

[1] M. D. Banea, M. Rosioara, R. J. C. Carbas, and L. F. M. da Silva, "Multi-material adhesive joints for automotive industry," *Compos. Part B Eng.*, vol. 151, no. May, pp. 71–77, 2018.

[2] F. J. P. Chaves, L. F. M. Da Silva, M. F. S. F. De Moura, D. A. Dillard, and V. H. C. Esteves, "Fracture mechanics tests in adhesively bonded joints: A literature

review," *J. Adhes.*, vol. 90, no. 12, pp. 955–992, 2014.

[3] A. J. Kinloch and S. O. Osiyemi, "Predicting the Fatigue Life of Adhesively-Bonded Joints," *J. Adhes.*, vol. 43, no. 1–2, pp. 79–90, 1993.

[4] W. Xu *et al.*, "Debonding monitoring of CFRP T-joint using optical acoustic emission sensor," *Compos. Struct.*, vol. 273, no. June, 2021.

[5] M. Rucka, E. Wojtczak, and J. Lachowicz, "Damage imaging in lamb wave-based inspection of adhesive joints," *Appl. Sci.*, vol. 8, no. 4, 2018.

[6] E. Siryabe, M. Renier, A. Meziane, and M. Castaings, "The transmission of lamb waves across adhesively bonded lap joints to evaluate interfacial adhesive properties," *Phys. Procedia*, vol. 70, pp. 541–544, 2015.

[7] W. Ostachowicz and M. Radzieński, "Structural health monitoring by means of elastic wave propagation," *J. Phys. Conf. Ser.*, vol. 382, no. 1, 2012.

[8] J. J. Moughty and J. R. Casas, "A state of the art review of modal-based damage detection in bridges: Development, challenges, and solutions," *Appl. Sci.*, vol. 7, no. 5, 2017.

[9] M. Saeedifar, M. A. Najafabadi, D. Zarouchas, H. H. Toudeshky, and M. Jalalvand, "Barely visible impact damage assessment in laminated composites using acoustic emission," *Compos. Part B Eng.*, vol. 152, no. June, pp. 180–192, 2018.

[10] M. Bourchak, I. R. Farrow, I. P. Bond, C. W. Rowland, and F. Menan, "Acoustic emission energy as a fatigue damage parameter for CFRP composites," *Int. J. Fatigue*, vol. 29, no. 3, pp. 457–470, 2007.

[11] M. Saeedifar, J. Mansvelder, R. Mohammadi, and D. Zarouchas, "Using passive and active acoustic methods for impact damage assessment of composite structures," *Compos. Struct.*, vol. 226, no. June, p. 111252, 2019.

[12] M. Saeedifar, M. N. Saleh, S. T. De Freitas, and D. Zarouchas, "Damage characterization of adhesively-bonded Bi-material joints using acoustic emission," *Compos. Part B Eng.*, vol. 176, no. August, p. 107356, 2019.

[13] J. Manterola, M. Aguirre, J. Zurbitu, J. Renart, A. Turon, and I. Urresti, "Using acoustic emissions (AE) to monitor mode I crack growth in bonded joints," *Eng. Fract. Mech.*, vol. 224, no. July 2019, p. 106778, 2020.

[14] M. G. Droubi, A. Stuart, J. Mowat, C. Noble, A. K. Prathuru, and N. H. Faisal, "Acoustic emission method to study fracture (Mode-I, II) and residual strength characteristics in composite-to-metal and metal-to-metal adhesively bonded joints," *J. Adhes.*, vol. 94, no. 5, pp. 347–386, 2018.

[15] R. A. A. Lima, M. Drobiazko, A. Bernasconi, and M. Carboni, "On crack tip localisation in quasi-statically loaded, adhesively bonded double cantilever beam specimens by acoustic emission," *Theor. Appl. Fract. Mech.*, vol. 118, no. February, p. 103286, 2022.

[16] M. Saeedifar and D. Zarouchas, "Damage characterization of laminated composites using acoustic emission: A review," *Compos. Part B Eng.*, vol. 195, no. January, p. 108039, 2020.

[17] M. Z. Sadeghi *et al.*, "Damage detection in adhesively bonded single lap joints by using backface strain: Proposing a new position for backface strain gauges," *Int. J. Adhes. Adhes.*, vol. 97, no. November, 2020.

[18] M. H. Kang, J. H. Choi, and J. H. Kweon, "Fatigue life evaluation and crack detection of the adhesive joint with carbon nanotubes," *Compos. Struct.*, vol. 108, no. 1, pp. 417–422, 2014.

[19] X. F. Sánchez-romate, C. Sbarufatti, and M. Sánchez, "Fatigue crack growth identi fi cation in bonded joints by using carbon nanotube doped adhesive fi lms."

[20] O. Sam-Daliri *et al.*, "Impedance analysis for condition monitoring of single lap CNT-epoxy adhesive joint," *Int. J. Adhes. Adhes.*, vol. 88, no. November 2018, pp. 59–65, 2019.

[21] R. Dugnani, Y. Zhuang, F. Kopsaftopoulos, and F. K. Chang, "Adhesive bond-line degradation detection via a cross-correlation electromechanical impedance–based approach," *Struct. Heal. Monit.*, vol. 15, no. 6, pp. 650–667, 2016.

[22] J. Weiland, M. Luber, R. Seewald, A. Schiebahn, R. Engelbrecht, and U. Reisgen,

"Structural health monitoring of adhesively bonded joints: Proposing a new method by use of polymer optical fibers," *Procedia Struct. Integr.*, vol. 28, no. 2019, pp. 1249–1257, 2020.

[23] L. Wong, N. Chowdhury, J. Wang, W. K. Chiu, and J. Kodikara, "Fatigue damage monitoring of a composite step lap joint using distributed optical fibre sensors," *Materials (Basel).*, vol. 9, no. 5, 2016.

[24] S. Sulejmani *et al.*, "Disbond monitoring in adhesive joints using shear stress optical fiber sensors," *Smart Mater. Struct.*, vol. 23, no. 7, 2014.

[25] M. G. R. Sause, "In Situ Monitoring of Fiber-Reinforced Composites," vol. 242, p. 633, 2016.

[26] J. Weiland, M. Z. Sadeghi, J. V. Thomalla, A. Schiebahn, K. U. Schroeder, and U. Reisgen, "Analysis of back-face strain measurement for adhesively bonded single lap joints using strain gauge, Digital Image Correlation and finite element method," *Int. J. Adhes. Adhes.*, vol. 97, no. November, p. 102491, 2020.

[27] A. Bernasconi, M. Carboni, L. Comolli, R. Galeazzi, A. Gianneo, and M. Kharshiduzzaman, "Fatigue crack growth monitoring in composite bonded lap joints by a distributed fibre optic sensing system and comparison with ultrasonic testing," *J. Adhes.*, vol. 92, no. 7–9, pp. 739–757, 2016.

[28] C. S. Shin, Y. J. Yang, and S. K. Liaw, "Monitoring fatigue damage of an adhesive joint using fiber optics sensors," *J. Phys. Conf. Ser.*, vol. 843, no. 1, 2017.

[29] O. Sam-Daliri, L. M. Faller, M. Farahani, and H. Zangl, "Structural health monitoring of adhesive joints under pure mode I loading using the electrical impedance measurement," *Eng. Fract. Mech.*, vol. 245, no. February, p. 107585, 2021.

[30] S. Masmoudi, A. El Mahi, S. Turki, and R. El Guerjouma, "Mechanical behavior and health monitoring by Acoustic Emission of unidirectional and cross-ply laminates integrated by piezoelectric implant," *Appl. Acoust.*, vol. 86, pp. 118–125, 2014.

[31] M. Drissi-Habti, V. Raman, A. Khadour, and S. Timorian, "Fiber optic sensor

embedment study for multi-parameter strain sensing," *Sensors (Switzerland)*, vol. 17, no. 4, pp. 1–16, 2017.

[32] R. A. A. A. A. Lima, R. Perrone, M. Carboni, and A. Bernasconi, "Experimental analysis of mode I crack propagation in adhesively bonded joints by optical backscatter reflectometry and comparison with digital image correlation," *Theor. Appl. Fract. Mech.*, vol. 116, no. July, p. 103117, Oct. 2021.

[33] T. Augustin, J. Karsten, and B. Fiedler, "Detection and localization of impact damages in carbon nanotube–modified epoxy adhesive films with printed circuits," *Struct. Heal. Monit.*, vol. 17, no. 5, pp. 1166–1177, 2018.

[34] H. Murayama, K. Kageyama, K. Uzawa, K. Ohara, and H. Igawa, "Strain monitoring of a single-lap joint with embedded fiber-optic distributed sensors," *Struct. Heal. Monit.*, vol. 11, no. 3, pp. 325–344, 2012.

[35] A. Stawiarski, M. Barski, and P. Pająk, "Fatigue crack detection and identification by the elastic wave propagation method," *Mech. Syst. Signal Process.*, vol. 89, pp. 119–130, 2017.

[36] T. Loutas, N. Eleftheroglou, and D. Zarouchas, "A data-driven probabilistic framework towards the in-situ prognostics of fatigue life of composites based on acoustic emission data," *Compos. Struct.*, vol. 161, pp. 522–529, 2017.

[37] N. Grundmann, H. Brüning, K. Tserpes, T. Strohbach, and B. Mayer, "Influence of embedding fiber optical sensors in cfrp film adhesive joints on bond strength," *Sensors (Switzerland)*, vol. 20, no. 6. 2020.

[38] M. Carboni and A. Bernasconi, *Acoustic Emission Based Monitoring of Fatigue Damage in CFRP-CFRP Adhesive Bonded Joints*, vol. 127. Springer International Publishing, 2021.

[39] A. Bernasconi, L. M. Martulli, and M. Carboni, "Fatigue crack growth analysis in composite bonded joints by back face distributed strain sensing and comparison with X-ray microtomography," *Int. J. Fatigue*, vol. 154, no. May 2021, p. 106526, 2022.

[40] N. Ben Salem, M. K. Budzik, J. Jumel, M. E. R. Shanahan, and F. Lavelle,

"Investigation of the crack front process zone in the double cantilever beam test with backface strain monitoring technique," *Eng. Fract. Mech.*, vol. 98, no. 1, pp. 272–283, 2013.

[41] Z. Zhang, J. K. Shang, F. V Lawrence Jr, and F. V. Lawrence, *A Backface Strain Technique for Detecting Fatigue Crack Initiation in Adhesive Joints*, vol. 49, no. 1–2. 1995, pp. 23–36.

[42] A. Graner Solana, A. D. Crocombe, and I. A. Ashcroft, "Fatigue life and backface strain predictions in adhesively bonded joints," *Int. J. Adhes. Adhes.*, vol. 30, no. 1, pp. 36–42, 2010.

[43] A. Bernasconi, M. Kharshiduzzaman, and L. Comolli, "Strain Profile Measurement for Structural Health Monitoring of Woven Carbon-fiber Reinforced Polymer Composite Bonded joints by Fiber Optic Sensing Using an Optical Backscatter Reflectometer," *J. Adhes.*, vol. 92, no. 6, pp. 440–458, 2016.

[44] V. Shenoy, I. A. Ashcroft, G. W. Critchlow, and A. D. Crocombe, "Unified methodology for the prediction of the fatigue behaviour of adhesively bonded joints," *Int. J. Fatigue*, vol. 32, no. 8, pp. 1278–1288, 2010.

[45] R. de A. A. Lima *et al.*, "Interfacial adhesion between embedded fibre optic sensors and epoxy matrix in composites," *J. Adhes. Sci. Technol.*, vol. 33, no. 3, pp. 253–272, 2019.

[46] R. Di Sante, "Fibre optic sensors for structural health monitoring of aircraft composite structures: Recent advances and applications," *Sensors (Switzerland)*, vol. 15, no. 8, pp. 18666–18713, 2015.

[47] N. Takeda, Y. Okabe, and T. Mizutani, "Damage detection in composites using optical fibre sensors," *Proc. Inst. Mech. Eng. Part G J. Aerosp. Eng.*, vol. 221, no. 4, pp. 497–508, 2007.

[48] L. F. M. Da Silva, P. M. G. P. Moreira, and A. L. D. Loureiro, "Determination of the strain distribution in adhesive joints using Fiber Bragg Grating (FBG)," *Journal of Adhesion Science and Technology*, vol. 28, no. 14–15. pp. 1480–1499, 2014.

[49] P. Bao, M. Yuan, S. Dong, H. Song, and J. Xueb, “Fiber Bragg grating sensor fatigue crack real-time monitoring based on spectrum cross-correlation analysis,” *J. Sound Vib.*, vol. 332, no. 1, pp. 43–57, 2013.

[50] A. Güemes and B. Soller, “Optical fiber distributed sensing: Physical principles and applications,” *Struct. Heal. Monit. 2009 From Syst. Integr. to Auton. Syst. - Proc. 7th Int. Work. Struct. Heal. Monit. IWSHM 2009*, vol. 1, no. 3, pp. 14–20, 2009.

[51] G. Galanopoulos, D. Milanoski, A. Broer, D. Zarouchas, and T. Loutas, “Health Monitoring of Aerospace Structures Utilizing Novel Health Indicators Extracted from Complex Strain and Acoustic Emission Data,” *Sensors*, vol. 21, no. 17, p. 5701, 2021.

[52] C. S. Shin and T. C. Lin, “Adhesive joint integrity monitoring using the full spectral response of fiber bragg grating sensors,” *Polymers*, vol. 13, no. 17. 2021.

[53] D. M. Peairs, L. Sterner, K. Flanagan, and V. Kochergin, “Fiber optic monitoring of structural composites using optical backscatter reflectometry,” *Int. SAMPE Tech. Conf.*, no. February, 2009.

[54] A. Gianneo, M. Carboni, and A. Bernasconi, “Crack profile reconstruction of cfrp-cfrp bonded joints from optical backscatter reflectometry and comparison with x-ray computed tomography,” *14th Int. Conf. Slov. Soc. Non-Destructive Test. "Application Contemp. Non-Destructive Test. Eng. Conf. Proc.*, vol. 2017-Septe, pp. 109–116, 2017.

[55] R. Sieńko, M. Zych, Ł. Bednarski, and T. Howiacki, “Strain and crack analysis within concrete members using distributed fibre optic sensors,” *Struct. Heal. Monit.*, vol. 18, no. 5–6, pp. 1510–1526, 2019.

[56] M. A. Bisyarin, O. I. Kotov, A. H. Hartog, L. B. Liokumovich, and N. A. Ushakov, “Rayleigh backscattering from the fundamental mode in step-index multimode optical fibers,” *Appl. Opt.*, vol. 56, no. 2, p. 354, 2017.

[57] A. Barrias, G. Rodriguez, J. R. Casas, and S. Villalba, “Application of distributed optical fiber sensors for the health monitoring of two real structures in Barcelona,”

Struct. Infrastruct. Eng., vol. 14, no. 7, pp. 967–985, 2018.

[58] M. F. Bado, J. R. Casas, and J. Gómez, "Post-processing algorithms for distributed optical fiber sensing in structural health monitoring applications," *Struct. Heal. Monit.*, 2020.

[59] S. Cardamone, A. Bernasconi, and M. Giglio, "Characterization of the 3M Scotch-Weld™ 7260 B/A epoxy adhesive by cohesive damage models and application to a full-scale bonded sub-structure," *J. Adhes.*, pp. 1–46, 2019.

[60] A. Bernasconi, R. A. A. Lima, S. Cardamone, R. B. Campbell, A. H. Slocum, and M. Giglio, "Effect of temperature on cohesive modelling of 3M Scotch-Weld™ 7260 B/A epoxy adhesive," *J. Adhes.*, vol. 96, no. 1–4, pp. 437–460, 2020.

[61] A. Bernasconi, M. Carboni, and L. Comolli, "Monitoring of fatigue crack growth in composite adhesively bonded joints using Fiber Bragg Gratings," *Procedia Eng.*, vol. 10, pp. 207–212, 2011.

[62] M. Zhu *et al.*, "Digital image correlation assisted characterization of Mode I fatigue delamination in composites," *Compos. Struct.*, vol. 253, no. November 2019, p. 112746, 2020.

[63] J. J. L. Morais *et al.*, "The double cantilever beam test applied to mode I fracture characterization of cortical bone tissue," *J. Mech. Behav. Biomed. Mater.*, vol. 3, no. 6, pp. 446–453, 2010.

[64] F. Sun and B. R. K. Blackman, "Using digital image correlation to automate the measurement of crack length and fracture energy in the mode I testing of structural adhesive joints," *Eng. Fract. Mech.*, vol. 255, no. June, p. 107957, 2021.

[65] M. Cabello, A. Turon, J. Zurbitu, J. Renart, C. Sarrado, and F. Martínez, "Progressive failure analysis of DCB bonded joints using a new elastic foundation coupled with a cohesive damage model," *Eur. J. Mech. A/Solids*, vol. 63, pp. 22–35, 2017.

[66] F. Sun and B. R. K. Blackman, "A DIC method to determine the Mode I energy release rate G, the J-integral and the traction-separation law simultaneously for adhesive joints," *Eng. Fract. Mech.*, vol. 234, no. December 2019, p. 107097,

2020.

[67] R. Mactabi, I. D. Rosca, and S. V. Hoa, “Monitoring the integrity of adhesive joints during fatigue loading using carbon nanotubes,” *Compos. Sci. Technol.*, vol. 78, pp. 1–9, 2013.

[68] M. J. Donough, A. J. Gunnion, A. C. Orifici, and C. H. Wang, “Plasticity induced crack closure in adhesively bonded joints under fatigue loading,” *Int. J. Fatigue*, vol. 70, pp. 440–450, 2015.

[69] S. Azari, G. Jhin, M. Papini, and J. K. Spelt, “Fatigue threshold and crack growth rate of adhesively bonded joints as a function of load/displacement ratio,” *Compos. Part A Appl. Sci. Manuf.*, vol. 57, pp. 59–66, 2014.

[70] I. Bello, Y. Alowayed, J. Albinmousa, G. Lubineau, and N. Merah, “Fatigue crack growth in laser-treated adhesively bonded composite joints: An experimental examination,” *Int. J. Adhes. Adhes.*, vol. 105, p. 102784, 2021.

[71] S. Azari, M. Papini, and J. K. Spelt, “Effect of adhesive thickness on fatigue and fracture of toughened epoxy joints - Part I: Experiments,” *Eng. Fract. Mech.*, vol. 78, no. 1, pp. 153–162, 2011.

[72] A. Pirondi and G. Nicoletto, “Fatigue crack growth in bonded DCB specimens,” *Eng. Fract. Mech.*, vol. 71, no. 4–6, pp. 859–871, 2004.

[73] M. V. Fernández, M. F. S. F. De Moura, L. F. M. Da Silva, and A. T. Marques, “Composite bonded joints under mode i fatigue loading,” *Int. J. Adhes. Adhes.*, vol. 31, no. 5, pp. 280–285, 2011.

[74] Q. Sourisseau, E. Lepretre, S. Chataigner, X. Chapeleau, L. Mouton, and S. Paboeuf, “Use of high spatial resolution distributed optical fiber to monitor the crack propagation of an adhesively bonded joint during ENF and DCB tests,” *Int. J. Adhes. Adhes.*, vol. 115, no. February, 2022.